PHYSICAL REVIEW D **83,** 103501 (2011)

# Large scale structure forecast constraints on particle production during inflation

Teeraparb Chantavat,* Christopher Gordon, and Joseph Silk
*Oxford Astrophysics, Denys Wilkinson Building, Keble Road, Oxford, OX1 3RH, United Kingdom*
(Received 13 October 2010; published 2 May 2011)

Bursts of particle production during inflation provide a well-motivated mechanism for creating bumplike features in the primordial power spectrum. Current data constrain these features to be less than about 5% the size of the featureless primordial power spectrum at wave numbers of about $0.1h$ Mpc$^{-1}$. We forecast that the Planck cosmic microwave background experiment will be able to strengthen this constraint to the 0.5% level. We also predict that adding data from a square kilometer array galaxy redshift survey would improve the constraint to about the 0.1% level. For features at larger wave numbers, Planck will be limited by Silk damping and foregrounds, while the square kilometer array will be limited by nonlinear effects. We forecast, for a cosmic inflation probe galaxy redshift survey, that similar constraints can be achieved up to about a wave number of $1.0h$ Mpc$^{-1}$.

DOI: 10.1103/PhysRevD.83.103501 PACS numbers: 98.80.−k

## I. INTRODUCTION

Current data are remarkably consistent with predictions of the simplest models of inflation. To a high degree of accuracy, the Universe appears to be flat and have nearly scale-invariant, isotropically distributed, Gaussian, and adiabatic primordial perturbations [1,2]. However, there are still potentially large improvements to be implemented in the precision and the length scales of the primordial perturbations that will be probed. Therefore, it is important to investigate possible deviations from this simple picture that may, in the future, be detectable. In this article, we concentrate on features in the primordial power spectrum that may be caused by bursts of particle production during inflation [3–5]. This can happen when the motion of the inflaton causes the mass of another field to pass through zero. The resultant production of particles leads to a corresponding bumplike feature in the primordial power spectrum at around the scales which are then leaving the Hubble horizon.

A feature in the primordial power will translate to a corresponding feature in the CMB angular power spectrum and the matter power spectrum. The matter power spectrum may be probed in many ways, and in this article we concentrate on galaxy redshift surveys and cluster surveys.

Currently, there is no detection of such features in the data, but only wave numbers of $k \lesssim 0.1h$ Mpc$^{-1}$ have been probed and only to accuracies of about 5% [3]. The Planck CMB survey can probe smaller length scales due to higher resolution and lower noise and so will help improve the constraints up to $k \sim 0.2h$ Mpc$^{-1}$, where noise, beam size limitations, and foregrounds start to dominate. In general, astrophysical foregrounds prevent one from probing the primordial power spectrum beyond about $k \sim 0.5h$ Mpc$^{-1}$ using the CMB. Future galaxy redshift surveys, such as those that are planned with the Square Kilometer Array[1] (SKA), will also probe $k \sim 0.1h$ Mpc$^{-1}$ to a much higher accuracy due to the huge volumes that they will encompass, but will be limited to $k \lesssim 0.2h$ Mpc$^{-1}$ by nonlinear effects. However, $k \lesssim 2h$ Mpc$^{-1}$ may be probed by very high redshift galaxy surveys, such as the Cosmic Inflation Probe[2] (CIP), where nonlinear growth has yet to dominate.

In this article, we will make forecasts on how well the amplitude of a particle production-induced feature can be constrained by future large-scale structure surveys. We begin in Sec. II with a summary of how particle production can generate a bumplike feature. In Sec. III, we give an overview of Fisher information matrices, a conventional method of predicting constraints on a set of parameters, for CMB, galaxy, and cluster surveys. Predictions for constraints on the feature amplitude and position combined with other cosmological parameters are given in Sec. IV. We discuss our results in Sec. V.

## II. PARTICLE PRODUCTION

Recently, a mechanism has been proposed that will generate a bumplike feature through particle production during inflation [3–5]. In this scenario, the production of massive isoinflaton particles during inflation gives rise to potentially quantitatively observable features in the primordial power spectrum. The fields simply interact via the coupling

$$\mathcal{L}_{\rm int} = -\frac{g_{\rm IR}^2}{2}(\phi - \phi_0)^2\chi^2, \tag{1}$$

where $g_{\rm IR}$ is the interaction coupling constant. $\phi$ and $\chi$ are the inflaton and isoinflaton fields, respectively. When $\phi$ passes through $\phi_0$ there is a nonadiabatic change in the mass of $\chi$ and, as a result, a burst of particle production.

*txc@astro.ox.ac.uk

[1]See http://www.skatelescope.org/.
[2]See http://www.cfa.harvard.edu/cip/.

 

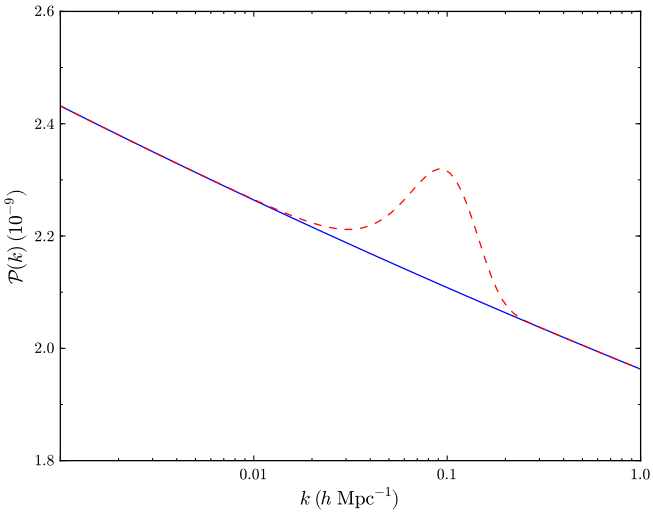


FIG. 1 (color online). The primordial power spectrum plus particle creation features with $A_{\rm IR} = 1.25 \times 10^{-10}$ at position $k_{\rm IR} = 0.1h$ Mpc$^{-1}$ (red dashed line).

This rapidly drains energy from the $\phi$ field, which can lead to a transient violation of slow roll and hence an associated "ringing" in the primordial curvature fluctuations which is similar to that seen in models with a sharp feature in the potential [6–14]. However, the dominant effect is found to come from multiple rescatterings of the produced $\delta\chi$ particles off the $\phi$ condensate. Multiple bumplike features are also possible with $\phi_0$'s in different positions, which is associated with different $g_{\rm IR}$'s. However, we restrict ourselves to the case where only one feature is present. The overall effect is a bumplike feature which can approximately be described by a parametric form as

$$\mathcal{P}(k) = \Delta^2_{\mathcal{R}}\left(\frac{k}{k_{\rm pivot}}\right)^{n_s-1} + A_{\rm IR}\left(\frac{\pi e}{3}\right)^{3/2} \times \left(\frac{k}{k_{\rm IR}}\right)^3 e^{-(\pi/2)(k/k_{\rm IR})^2}, \quad (2)$$

where $\Delta^2_{\mathcal{R}}$ is the scalar amplitude describing the normalization of the power spectrum. $n_s$ and $k_{\rm pivot}$ are the tilt and the pivot wave number respectively. The first term on the right-hand side of Eq. (2) is the standard power-law power spectrum and the second term contains the features generated by particle creation which is parametrized by an amplitude $A_{\rm IR}$ and position $k_{\rm IR}$, as shown in Fig. 1. The normalization is chosen so that $A_{\rm IR}$ is the amplitude of the feature at its peak $k_{\rm IR}$. The relation to the coupling constant is given by

$$A_{\rm IR} \approx 1.01 \times 10^{-6} g_{\rm IR}^{15/4}. \quad (3)$$

## III. FISHER MATRIX CALCULATION

We use the Fisher information matrix [15] to make predictions for constraints of cosmological parameters for future surveys. The statistics that will be implemented are cluster number counts, the cluster/galaxy power spectrum, and the cosmic microwave background power spectrum.

### A. Cluster number count

The simplest statistics we can extract from a cluster survey is the number count.

#### *1. Differential halo mass function*

In order to predict the number density of collapsed objects in the Universe, a statistical concept of halo or mass distribution is used here. The differential halo mass function, or halo mass function for short, is defined as the redshift-dependent distribution of the number of collapsed dark matter halos per unit mass interval in a unit comoving volume. The halo mass function is given by

$$\frac{dn}{dM} = \frac{\rho_m}{M}\frac{d\ln\sigma^{-1}}{dM} f(\sigma), \quad (4)$$

where $dn/dM$ is the differential halo mass function, $\rho_m$ is the matter density, and $f(\sigma)$ is called the mass fraction. The smoothed variance is calculated as

$$\sigma^2(R, z) = \frac{D(z)^2}{2\pi^2}\int_0^\infty P(k)W^2(k, R)k^2 dk, \quad (5)$$

where $D(z)$ is the linear growth function normalized to 1 at the present epoch. $W(k, R)$ is the Fourier-space top-hat window function. $R$ is the smoothing radius for a comoving sphere enclosing a mass of

$$M = \frac{4\pi}{3}R^3\rho_m = 1.16 \times 10^{12}\Omega_m\left(\frac{R}{h^{-1}\ {\rm Mpc}}\right)^3 h^{-1}M_\odot. \quad (6)$$

The top-hat smoothing in Eq. (5) suppresses the contribution of any change to the primordial power spectrum located at wave number $k_{\rm IR} \gg 1/R$. Combined with Eq. (6), this implies that a change in the primordial power spectrum at $k_{\rm IR}$ has a suppressed effect on the number density on mass scales satisfying

$$\frac{M}{h^{-1}M_\odot} \gg 10^{12}\left(\frac{k_{\rm IR}}{h\ {\rm Mpc}^{-1}}\right)^{-3}. \quad (7)$$

The mass fraction is defined as a fraction of mass in collapsed halos per unit interval in $\ln\sigma^{-1}$. The halo mass function is described by a pair of parameters, $f(\sigma)$ and $\ln\sigma^{-1}$. Each of these parameters gives a natural way of parametrizing the mass function from different cosmological models with the fewest number of parameters. All the cosmological parameters are embedded in $\sigma$. $f(\sigma)$ is the fraction of the density fluctuation that eventually collapses into nonlinear objects. We used the mass function by Jenkins *et al.* [16]:

$$f(\sigma) = 0.315 \exp[-|\ln\sigma^{-1} + 0.61|^{3.8}]. \quad (8)$$

#### 2. Number count Fisher matrix

For a survey, which covers a $f_{\rm sky}$ fraction of the sky, a theoretically expected value of the number of clusters in the $i$th redshift bin at central redshift $z_i$ and a width of $\Delta z$ is given by

$$\bar{N}(M > M_{\rm lim}, z) = f_{\rm sky} \int_{z_i-(1/2)\Delta z}^{z_i+(1/2)\Delta z} dz \frac{dV}{dz} \int_{M_{\rm lim}}^{\infty} dM \frac{dn}{dM}(M, z). \quad (9)$$

The differential comoving volume $dV/dz$ is

$$\frac{dV}{dz} = \frac{4\pi}{H(z)} \left[\int_0^z \frac{dz'}{H(z')}\right]^2, \quad (10)$$

where $H(z)$ is the Hubble parameter at redshift $z$. Equation (9) includes all the clusters above a threshold mass of $M_{\rm lim}$. The mass threshold can, in general, be redshift dependent, which is normally given in terms of a survey-specific selection function. To investigate generally how cluster surveys can be used to probe features, we will use a simple redshift-independent effective mass threshold for cluster surveys which yields an equivalent number of clusters over the entire survey volume.

Given a set of parameters of interest, $\Theta = (\theta_1, \theta_2, \ldots, \theta_m)$, an element $\theta_\mu$ and $\theta_\nu$ of a Fisher matrix for number count is [17]

$$F_{\mu\nu} = \sum_{i=1}^{N_{\rm bins}} \frac{1}{\bar{N}_i} \frac{\partial \bar{N}_i}{\partial \theta_\mu} \frac{\partial \bar{N}_i}{\partial \theta_\nu}, \quad (11)$$

where $F_{\mu\nu}$ is a sum of all redshift bins in the survey.

### B. Power spectrum

We also consider cosmological constraints from measurements of the matter power spectrum.

#### 1. Galaxy power spectrum

Galaxies are moving away from us along with the Hubble flow. The perturbation of the velocity of the galaxies is called the peculiar velocity, which is the motion of the galaxies relative to the Hubble flow. It changes the observed Doppler shift and, hence, the distance inferred from the redshift measurement. Kaiser [18] showed that the power spectrum derived from a redshift survey, $P_s(\mathbf{k})$, is given by

$$P_s(k, \mu) = [1 + \beta\mu^2]^2 b^2 P(k), \quad (12)$$

where $P(k)$ and $P_s(k)$ are the matter power spectrum and the redshift power spectrum, respectively, $\mu \equiv \hat{\mathbf{k}} \cdot \hat{\mathbf{n}}$ is the cosine of the angle between $\mathbf{k}$ and the line of sight, $\beta$ is

$$\beta = \frac{1}{b} \frac{d\ln D}{d\ln a}, \quad (13)$$

where $D$ is the linear growth function normalized to 1 at the present epoch, and $b \equiv \delta_g/\delta$ is the galaxy bias. The bias for galaxy surveys is normally estimated from the data, and the uncertainty in the bias is propagated into the other parameter constraints. However, to include nonlinear effects, we applied a Taylor-like expansion to the bias as

$$b^2 = b_0^2[1 + a_1 k + a_2 k^2], \quad (14)$$

where $b_0$ is a scale-independent bias. $a_1$ and $a_2$ are the first and second order terms, respectively [19].

The linear theory matter power spectrum is related to the primordial power spectrum by

$$P(k) \propto T^2(k) k \mathcal{P}(k), \quad (15)$$

where $T$ is the transfer function. So a narrow feature in the primordial power spectrum will be transferred to a narrow feature in the matter power spectrum at about the same comoving wave number; see Fig. 2.

#### 2. Cluster power spectrum

The Poisson approximation for cluster number counts is not strictly accurate for larger surveys [20]. There is an additional sample variance which can be used to help constrain the mass scaling relation. We account for this by incorporating an additional constraint from the power spectrum of the clusters. The way of doing this is similar to that for galaxies. However, in the case of the cluster bias, we use an effective linear halo bias

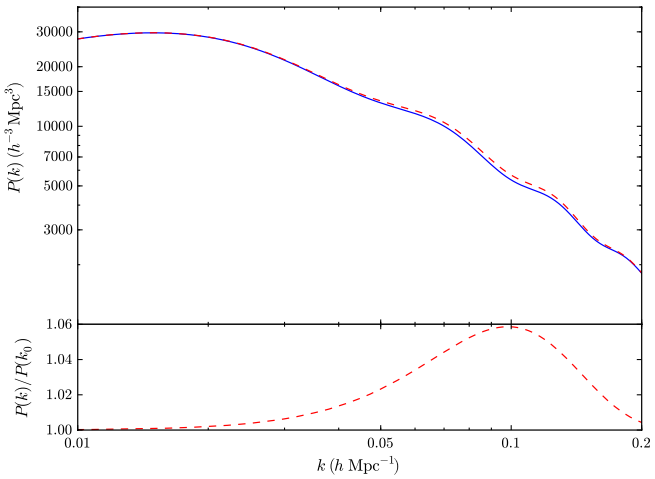


FIG. 2 (color online). The matter power spectrum from a featureless primordial power spectrum (blue solid line) and the matter power spectrum from a primordial power spectrum which has a particle creation feature with amplitude $A_{\rm IR} = 1.25 \times 10^{-10}$ at position $k_{\rm IR} = 0.1h$ Mpc$^{-1}$ (red dashed line).

$$b_{\rm eff}(z) = \frac{\int_{M_{\rm lim}}^{\infty} dM b(M,z) dn/dM}{\int_{M_{\rm lim}}^{\infty} dM dn/dM}, \quad (16)$$

where $dn/dM$ is the differential mass function [see Eq. (4)] and $b(M, z)$ can be calculated from the halo bias [21],

$$b(\nu) = 1 + \frac{a\nu - 1}{\delta_c} + \frac{2p}{\delta_c[1 + (a\nu)^p]}, \quad (17)$$

where $\nu = (\delta_c/\sigma)^2$ with $\delta_c = 1.69$, $a = 0.75$, and $p = 0.3$.

#### 3. Power spectrum Fisher matrix

We may write the appropriate Fisher matrix for the power spectrum by assuming the likelihood function to be Gaussian as [22]

$$F_{\mu\nu} = \frac{1}{2}\int_{k_{\rm min}}^{k_{\rm max}} \frac{d^3\mathbf{k}}{(2\pi)^3} \frac{\partial \ln P_s(\mathbf{k})}{\partial\theta_\mu} V_{\rm eff}(\mathbf{k}) \frac{\partial \ln P_s(\mathbf{k})}{\partial\theta_\nu}. \quad (18)$$

We set $k_{\rm max}$ to be the wave number, where nonlinear effects start to become non-negligible [23], where $\sigma(R_{\rm nl}) = 0.5$ and $k_{\rm max} = k_{\rm nl} = \pi/2/R_{\rm nl}$. We set $k_{\rm min} = 1.0 \times 10^{-4}$ Mpc$^{-1}$ for the lower limit. The effective survey volume $V_{\rm eff}$ is given by

$$V_{\rm eff}(k,\mu) = \int d^3\mathbf{r}\left[\frac{n(\mathbf{r})P_s(k,\mu)}{n(\mathbf{r})P_s(k,\mu)+1}\right]^2 \approx \left[\frac{\bar{n}P_s(k,\mu)}{\bar{n}P_s(k,\mu)+1}\right]^2 V_{\rm survey}, \quad (19)$$

where $n(\mathbf{r})$ is the number density at position $\mathbf{r}$ and $\bar{n}$ is the average number density for the survey. The effective volume is due to a finite survey volume and incomplete sampling of the underlying density field. These are known as sample variance and shot noise, respectively. The uncertainty is propagated through the calculation by the weighing factor $[n(\mathbf{r})P_s/(n(\mathbf{r})P_s + 1)]^2$. For galaxy surveys where the number density is high, i.e. $\bar{n}P_s(k,\mu) \gg 1$, the effective survey volume is then $V_{\rm eff} \approx V_{\rm survey}$.

### C. CMB

The primordial power spectrum is probed over a wide range of wave numbers by measurements of the primary CMB anisotropies (see, for example, [24]). Both the temperature ($T$) and $E$-mode of the polarization ($E$) probe scalar perturbations.

$$\frac{\ell(\ell+1)C_\ell^X}{2\pi} = \int d\ln k (T_\ell^X(k))^2 \mathcal{P}(k), \quad (20)$$

where $X \in T, E$ for the autocorrelation function ($TT$, $EE$). For the cross-correlation power spectrum ($TE$),

$$\frac{\ell(\ell+1)C_\ell^C}{2\pi} = \int d\ln k T_\ell^T(k) T_\ell^E(k) \mathcal{P}(k). \quad (21)$$

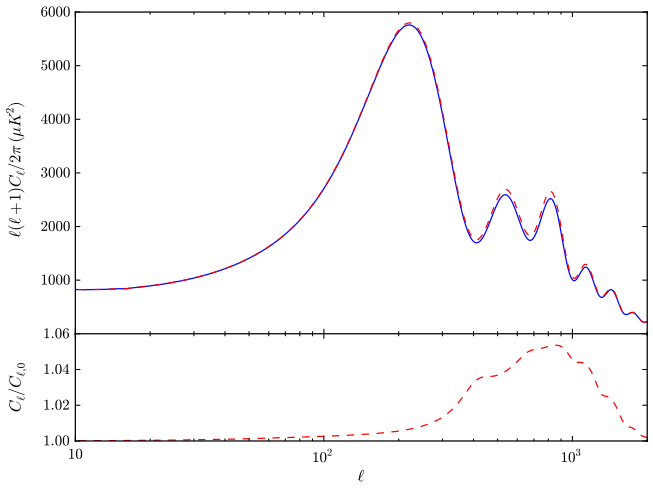


FIG. 3 (color online). The CMB angular power spectrum from a featureless primordial power spectrum (blue solid line) and the CMB angular power spectrum from a primordial power spectrum with a particle creation feature which has $A_{\rm IR} = 1.25 \times 10^{-10}$ at position $k_{\rm IR} = 0.1h$ Mpc$^{-1}$ (red dashed line).

The projection of a mode of wave number $k$ onto the surface of last scattering (a sphere of comoving radius $D_*$) results in the CMB transfer functions having the form $T_\ell^X \sim j_\ell(kD_*)$, where $j_\ell$ is the spherical Bessel function of order $\ell$ which peaks at $\ell \approx kD_*$. Therefore, a bump in the primordial power spectrum at wave number $k_i$ is mapped onto a bump in the CMB angular power spectrum at

$$\ell \sim k_{\rm IR}D_* \approx 10^4 \frac{k_{\rm IR}}{h\ {\rm Mpc}^{-1}}; \quad (22)$$

see Fig. 3.

The foreground contribution from secondary sources will probably be hard to completely remove for $\ell > 2000$ for both temperature and polarization. For this reason, as done by [24,25], we will restrict ourselves to $\ell \leq 2000$ when evaluating the forecasted marginalized errors.

The CMB Fisher matrix is given by (see, for example, [26])

$$F_{ij} = \sum_\ell \sum_{X,X'} \frac{\partial C_\ell^X}{\partial\theta_i} {\rm Cov}^{-1}(C_\ell^X, C_\ell^{X'}) \frac{\partial C_\ell^{X'}}{\partial\theta_j}, \quad (23)$$

where the covariance matrix can be obtained from [26] and it depends on the temperature noise per pixel ($\sigma_T$), the polarization noise per pixel ($\sigma_E$), the pixel area in radians squared ($\theta^2 = 4\pi/N_{\rm pix}$), and the beam window function which we approximate as Gaussian [$B_\ell \approx \exp(-\ell(\ell+1)\sigma_b^2$].

## IV. FORECAST CONSTRAINTS

With the descriptions of Fisher information matrices in Sec. III, we can make predictions for upcoming surveys. We also test our Fisher matrix formalism on some current surveys and compare to published results. For the CMB we

TABLE I. Planck instrument characteristics.

| Center frequency (GHz) | 70 | 100 | 143 | 217 |
|---|---|---|---|---|
| $\theta$ (FWHM arcmin) | 14 | 10 | 7.1 | 5.0 |
| $\sigma_T$ ($\mu$K) | 12.8 | 6.8 | 6.0 | 13.1 |
| $\sigma_E$ ($\mu$K) | 18.2 | 10.9 | 11.4 | 26.7 |

take the Planck[3] and Wilkinson microwave anisotropy probe (WMAP)[4] surveys. The values for Planck are taken from the Planck Blue Book[5] and are listed in Table I (note that $\theta$ needs to be converted to radians). We use $\sigma_b = \theta/\sqrt{8\log 2}$ and combine the different frequency bands as specified in [27]. We take the range in $\ell$ to be 2 to 2000. At higher $\ell$, secondary sources of temperature and polarization will likely prohibit the extraction of cosmological information from the primary CMB.

For galaxy surveys, we consider the CIP [28], which is a space-based mission aimed to measure the linear galaxy power spectrum over $k \sim 0.03$–$2.0h$ Mpc$^{-1}$ to better than 1%. The primary science goal of the CIP is to provide constraints on inflation models by observing $H\alpha$. The CIP survey will cover 1000 square degrees and will be capable of detecting more than $10^8$ galaxies in the redshift range of 1.8–6.5. We follow the CIP model by having redshift bins at $z = 2.0$–$3.5$, 3.5–5.0, and 5.0–6.5, and by having average galaxy number densities of $1.0 \times 10^{-2}$, $5.3 \times 10^{-3}$, and $1.3 \times 10^{-3} h^3$ Mpc$^{-3}$, respectively, which is equivalent to $\sim 1 \times 10^8$ galaxies within the survey volume of $\sim 15.0 h^{-3}$ Gpc$^3$. We restrict our calculation to $k_{\max} = 0.5$, 1.0, and $2.0h$ Mpc$^{-1}$ for the three bins, respectively [see Eq. (18)].

The Sloan Digital Sky Survey[6] (SDSS) [29] is a ground-based optical survey using a 2.5 m telescope at the Apache Point Observatory, New Mexico. Its final data set (DR7) includes more than $230 \times 10^6$ celestial objects and spectra of about 930 000 galaxies and 120 000 quasars over an area of 8400 square degrees in five optical band passes to a redshift of about 1.0. We follow the SDSS survey model from Pritchard and Pierpaoli [30]. We estimate the bias for the SDSS survey as 2.25 (i.e. $b \equiv \sigma_{8,g}/\sigma_8$, where $\sigma_{8,g} = 1.8$ and $\sigma_8 = 0.8$) and $\bar{n} = 1.0 \times 10^{-4} h^3$ Mpc$^{-3}$. The SKA is a large-scale radio telescope which aims to cover the frequency range from 60 MHz to 35 GHz as well as 20 000 square degrees of the sky. The main science goal of the SKA project is to study the HI content of galaxies to cosmologically significant distances, $z \sim 2.0$, and to make reionization maps using a 21 cm transition of neutral hydrogen. The SKA project is currently in a design phase, and the telescope site will be decided in 2012. We consider the galaxy redshift survey component of SKA (see, for example, [31]). It may also be possible to use the 21 cm absorption component of the SKA to probe reionization and the matter power spectrum at a higher redshift (see, for example, [32]). We shall consider the SKA survey as a stereotype of a cosmic variance-limited galaxy redshift survey by assuming that the number density is so high that $\bar{n}P_s \gg 1.0$. Hence, the effective survey volume is equivalent to the survey volume [see Eq. (19)] from $z = 0.0$–$2.0$. The set of parameters of all the galaxy surveys will include bias as an additional parameter, reflecting the fact that we do not accurately know the value of the bias. The uncertainty in bias will propagate into the parameter constraints.

For cluster surveys, we consider an all-sky extended Roentgen survey with an imaging telescope array[7] (eROSITA) which is a high sensitivity all-sky x-ray survey in the 0.2–12 keV energy band. The key science goal for eROSITA is to constrain the properties of dark energy using high redshift clusters of galaxies. It will have the capability to measure the spatial correlation features and evolution of a sample of about 50 000 galaxy clusters over a redshift range of 0.0–2.0 and will be able to find collapsed objects with mass above $3.5 \times 10^{14} h^{-1} M_\odot$. Our calculation of the expected cluster counts is in good agreement with the all-sky eROSITA cluster count given in the eROSITA documentation. We model the eROSITA survey by having $\Delta z = 0.2$ and $z = 0.0$–$2.0$. We also assume a 10% prior on the mass threshold determination for the eROSITA survey. The set of parameters of eROSITA will include the mass threshold as an additional parameter, reflecting the fact that we do not accurately know the mass of a cluster. The uncertainty in mass threshold will propagate into the parameter constraints.

The SuperNova/Acceleration Probe[8] (SNAP) survey [33,34] is a space-based experiment aiming to study dark energy and dark matter. We forecast the SNAP cluster lensing survey constraints [35] (see also [36–39]). Here we take $z = 0.0$–$1.4$, $\Delta z = 0.2$, $f_{\rm sky} = 0.024$, and a mass limit of $10^{14} h^{-1} M_\odot$. This roughly matches the number of clusters found using the more accurate selection function of [35] when we use their fiducial model cosmological parameters. Also, [38] found that the signal-to-noise ratio of a more realistic selection function was about the same as taking a mass limit of $10^{14} h^{-1} M_\odot$. Our SNAP selection function is biased to slightly higher redshifts than that of [35], but we expect this not to alter our predicted constraints significantly. We do not include the mass threshold into our analysis for the SNAP weak lensing survey, as the weak lensing technique can be used to determine the cluster mass accurately.

[3]See http://www.rssd.esa.int/index.php?project=planck.
[4]See http://map.gsfc.nasa.gov/.
[5]See http://www.rssd.esa.int/SA/PLANCK/docs/Bluebook-ESA-SCI(2005)1_V2.pdf.
[6]See http://www.sdss.org/.
[7]See http://www.mpe.mpg.de/heg/www/Projects/EROSITA/main.html.
[8]See http://snap.lbl.gov.

TABLE II. Details for galaxy and cluster surveys.

| Survey | $z$ | $\Delta z_{\rm bin}$ | $V_{\rm survey}(h^{-3}\ {\rm Gpc}^3)$ | $k_{\rm max}(h\ {\rm Mpc}^{-1})$ | $b$ | $M_{\rm lim}(h^{-1}M_\odot)$ | $f_{\rm sky}$ |
|---|---|---|---|---|---|---|---|
| Galaxy survey | | | | | | | |
| CIP | 2.0–6.5 | 1.5 | 15.0 | 2.0 | 1.0 | N/A | 0.024 |
| SDSS | 0.0–0.6 | 0.6 | 1.0 | 0.1 | 2.25 | N/A | 0.3 |
| SKA | 0.0–2.0 | 2.0 | 100 | 0.4 | 1.0 | N/A | 0.5 |
| Cluster survey | | | | | $(b_{\rm eff})$ | | |
| SNAP | 0.0–1.4 | 0.2 | 2.76 | 0.15 | 2.0 | $1.0\times10^{14}$ | 0.024 |
| eROSITA | 0.0–2.0 | 0.2 | 220 | 0.2 | 9.0 | $3.5\times10^{14}$ | 1.0 |

TABLE III. Constraints on fiducial cosmology.

| Survey | $\sigma_{\omega_b}$ | $\sigma_{\omega_c}$ | $\sigma_{\Omega_\Lambda}$ | $\sigma_{n_s}$ | $\sigma_{\alpha_s}$ | $\sigma_{\Delta^2_{\mathcal{R}}}(\times10^{-9})$ | $\sigma_\tau$ | $\sigma_{M_{\rm lim}}(\times10^{14}h^{-1}M_\odot)$ | $\sigma_b$ | $\sigma_{a_1}(h^{-1}\ {\rm Mpc})$ | $\sigma_{a_2}(h^{-2}\ {\rm Mpc}^2)$ |
|---|---|---|---|---|---|---|---|---|---|---|---|
| Galaxy survey | | | | | | | | | | | |
| CIP | 0.0022 | 0.0086 | 0.0043 | 0.027 | 0.0082 | 0.23 | N/A | N/A | 0.0057 | 0.039 | 0.024 |
| CIP + WMAP | 0.000 26 | 0.000 70 | 0.0015 | 0.0047 | 0.0037 | 0.024 | 0.0068 | N/A | 0.0055 | 0.037 | 0.021 |
| CIP + Planck | 0.000 099 | 0.000 26 | 0.0012 | 0.0020 | 0.0032 | 0.013 | 0.0030 | N/A | 0.0043 | 0.029 | 0.019 |
| SDSS + WMAP | 0.000 46 | 0.0036 | 0.020 | 0.021 | 0.017 | 0.055 | 0.012 | N/A | 0.17 | 4.44 | 32.89 |
| SDSS + Planck | 0.000 13 | 0.0010 | 0.0055 | 0.0031 | 0.0049 | 0.020 | 0.0044 | N/A | 0.15 | 4.33 | 32.82 |
| SKA | 0.000 64 | 0.0028 | 0.0016 | 0.0096 | 0.0033 | 0.077 | N/A | N/A | 0.0029 | 0.028 | 0.041 |
| SKA + WMAP | 0.000 17 | 0.000 61 | 0.000 55 | 0.0028 | 0.0020 | 0.018 | 0.0055 | N/A | 0.0025 | 0.026 | 0.037 |
| SKA + Planck | 0.000 082 | 0.000 16 | 0.000 35 | 0.0016 | 0.0019 | 0.0069 | 0.0018 | N/A | 0.0022 | 0.022 | 0.032 |
| Cluster survey | | | | | | | | | | | |
| eROSITA + WMAP | 0.000 37 | 0.0021 | 0.011 | 0.013 | 0.0082 | 0.046 | 0.011 | 0.19 | N/A | N/A | N/A |
| eROSITA + Planck | 0.000 13 | 0.001 | 0.0052 | 0.003 | 0.0041 | 0.020 | 0.0043 | 0.09 | N/A | N/A | N/A |
| SNAP + WMAP | 0.000 39 | 0.0017 | 0.010 | 0.017 | 0.015 | 0.042 | 0.010 | N/A | N/A | N/A | N/A |
| SNAP + Planck | 0.000 12 | 0.000 66 | 0.0036 | 0.0027 | 0.0049 | 0.018 | 0.0042 | N/A | N/A | N/A | N/A |
| CMB | | | | | | | | | | | |
| WMAP | 0.0006 | 0.0057 | 0.032 | 0.030 | 0.021 | 0.06 | 0.012 | N/A | N/A | N/A | N/A |
| Planck | 0.000 13 | 0.0011 | 0.0057 | 0.0031 | 0.0049 | 0.02 | 0.004 | N/A | N/A | N/A | N/A |

A summary of all galaxy and cluster survey parameters is given in Table II. We combined both statistical measurements from cluster number counts and the power spectrum in our predictions for the eROSITA and SNAP surveys. For the cluster surveys, we estimated the effective bias using Eq. (16).

We follow the work done by Barnaby and Huang [3], who found a 2-$\sigma$ constraint on the amplitude of the feature of about $2.5\times10^{-10}$ on a scale of $k\sim0.006$–$0.1h\ {\rm Mpc}^{-1}$. We conservatively define our fiducial value for the amplitude as $A_{\rm IR}=1.25\times10^{-10}$ and the feature at positions $k_{\rm IR}=0.1$, 0.4 and $1.0h\ {\rm Mpc}^{-1}$. A survey $k_{\rm max}$ limits the range of feature positions it can probe. The SDSS and SKA surveys can only probe the feature at $k=0.1h\ {\rm Mpc}^{-1}$, while CIP is the deepest survey that can probe all of the above feature positions. The eROSITA and SNAP surveys probe only the $k=0.1h\ {\rm Mpc}^{-1}$ and $k=0.4h\ {\rm Mpc}^{-1}$ features, whereas the latter is probed by the number count component.

We define our fiducial set of parameters as the flat $\Lambda$CDM set of parameters with running of the spectral index, $\alpha_s$, plus the amplitude and the position of the feature $\Theta=(\omega_b,\omega_c,\Omega_\Lambda,n_s,\alpha_s,\Delta^2_{\mathcal{R}},\tau)=(0.0227,0.1107,0.738,0.969,0.0,2.15\times10^{-9},0.086)$ and $k_{\rm pivot}=0.05\ {\rm Mpc}^{-1}$. Our fiducial cosmological parameters are consistent with the WMAP7 maximum likelihood values [2], although their $k_{\rm pivot}=0.002\ {\rm Mpc}^{-1}$. We assume a negligible neutrino mass, but we checked that adding a non-negligible mass would not significantly change our results. The constraints for the fiducial parameters without a feature are given in Table III. For features, we show the marginalized constraints on $A_{\rm IR}$, $k_{\rm IR}$, $n_s$, and $\alpha_s$ in Tables IV, V, and VI for features at $k_{\rm IR}=0.1$, 0.4, and $1.0h\ {\rm Mpc}^{-1}$, respectively. The other cosmological parameters are included in the marginalization, but they are not particularly degenerate with the features. We use a modified version of the CAMB package[9] [40] to generate the power spectrum for our analysis.

[9]See http://camb.info/.

TABLE IV. Forecasted 1-$\sigma$ marginalized uncertainties for fiducial $k_{\rm IR} = 0.1h$ Mpc$^{-1}$, $A_{\rm IR} = 0.125 \times 10^{-9}$.

| Survey | $\sigma_{A_{\rm IR}}(\times 10^{-9})$ | $\sigma_{k_{\rm IR}}(h$ Mpc$^{-1})$ | $\sigma_{n_s}$ | $\sigma_{\alpha_s}$ |
|---|---|---|---|---|
| Galaxy survey | | | | |
| CIP | 0.016 | 0.0037 | 0.027 | 0.0083 |
| CIP + WMAP | 0.0085 | 0.0024 | 0.0047 | 0.0038 |
| CIP + Planck | 0.0066 | 0.0015 | 0.0024 | 0.0034 |
| SDSS + WMAP | 0.18 | 0.027 | 0.063 | 0.034 |
| SDSS + Planck | 0.013 | 0.0023 | 0.0043 | 0.0079 |
| SKA | 0.0039 | 0.0016 | 0.0083 | 0.0049 |
| SKA + WMAP | 0.0032 | 0.0014 | 0.0030 | 0.0026 |
| SKA + Planck | 0.0030 | 0.0010 | 0.0016 | 0.0023 |
| Cluster survey | | | | |
| eROSITA + WMAP | 0.10 | 0.025 | 0.033 | 0.015 |
| eROSITA + Planck | 0.011 | 0.0022 | 0.0040 | 0.0057 |
| SNAP + WMAP | 0.075 | 0.027 | 0.038 | 0.025 |
| SNAP + Planck | 0.012 | 0.0023 | 0.0038 | 0.0075 |
| CMB | | | | |
| WMAP | 0.19 | 0.027 | 0.064 | 0.035 |
| Planck | 0.013 | 0.0023 | 0.0044 | 0.0079 |

TABLE V. Forecasted 1-$\sigma$ marginalized uncertainties for fiducial $k_{\rm IR} = 0.4h$ Mpc$^{-1}$, $A_{\rm IR} = 0.125 \times 10^{-9}$.

| Survey | $\sigma_{A_{\rm IR}}(\times 10^{-9})$ | $\sigma_{k_{\rm IR}}(h$ Mpc$^{-1})$ | $\sigma_{n_s}$ | $\sigma_{\alpha_s}$ |
|---|---|---|---|---|
| Galaxy survey | | | | |
| CIP | 0.017 | 0.015 | 0.026 | 0.0084 |
| CIP + WMAP | 0.0075 | 0.0070 | 0.0048 | 0.0039 |
| CIP + Planck | 0.0072 | 0.0066 | 0.0021 | 0.0033 |

TABLE VI. Forecasted 1-$\sigma$ marginalized uncertainties for fiducial $k_{\rm IR} = 1.0h$ Mpc$^{-1}$, $A_{\rm IR} = 0.125 \times 10^{-9}$.

| Survey | $\sigma_{A_{\rm IR}}(\times 10^{-9})$ | $\sigma_{k_{\rm IR}}(h$ Mpc$^{-1})$ | $\sigma_{n_s}$ | $\sigma_{\alpha_s}$ |
|---|---|---|---|---|
| Galaxy survey | | | | |
| CIP | 0.031 | 0.096 | 0.027 | 0.0096 |
| CIP + WMAP | 0.023 | 0.087 | 0.0046 | 0.0043 |
| CIP + Planck | 0.022 | 0.086 | 0.0020 | 0.0036 |

## V. DISCUSSION

For the standard cosmology, our cosmological constraints are in good agreement with previous work. For example, our CIP constraints for $n_s$ and $\alpha_s$ are consistent with [32,41], and our results for SDSS and SKA are consistent with [30]. Our best constraint for $(n_s, \alpha_s)$ derives from CIP + Planck and SKA + Planck, which are (0.0020, 0.0032) and (0.0016, 0.0019), respectively. However, since CIP and SKA surveys probe the power spectrum at exclusively different redshift ranges, we can consider them as two independent surveys. The combined CIP + SKA + Planck improves the constraints to (0.0014, 0.0017).

From Tables IV, V, and VI, we investigate the effect of a feature on cosmological parameters on scales $k = 0.1$, 0.4, and $1.0h$ Mpc$^{-1}$, respectively. The WMAP + SDSS constraints for the $0.1h$ Mpc$^{-1}$ feature are consistent with those found for the actual data [3]. As the CMB is limited to $\ell \leq 2000$, it can only directly constrain the $k = 0.1h$ Mpc$^{-1}$ feature. It may be possible to extend this range somewhat for polarization, but probably not enough to completely encompass the width of the $0.4h$ Mpc$^{-1}$ centered feature. The cluster surveys were only able to help directly constrain the feature at $0.1h$ Mpc$^{-1}$. Although in previous work [42], we found that cluster surveys could constrain the primordial power spectrum directly at scales of $0.4h$ Mpc$^{-1}$, this was for a linear piecewise binning of the primordial power spectrum where the location of the feature did not need to be constrained.

With features at different positions, the constraint on $n_s$ remains almost the same, while the constraints on $\alpha_s$ are worsened by about a factor of 2. The degeneracies between $A_{\rm IR}$ and $k_{\rm IR}$ have a significant impact on the running as a variation in $\alpha_s$ could be made on a more localized scale than a variation in $n_s$. However, there is more of an improvement on $\alpha_s$ with CIP + Planck. Figure 4 shows that CIP could be used to break the degeneracy between $A_{\rm IR}$ and $\alpha_s$, while SKA only provides a tightened constraint but the degeneracy is still in the same direction. CIP is in a different direction as it has most of its constraining power at higher $k$ values and so the degeneracy between $A_{\rm IR}$, $\Delta^2_{\mathcal{R}}$, and $\alpha_s$ is different.

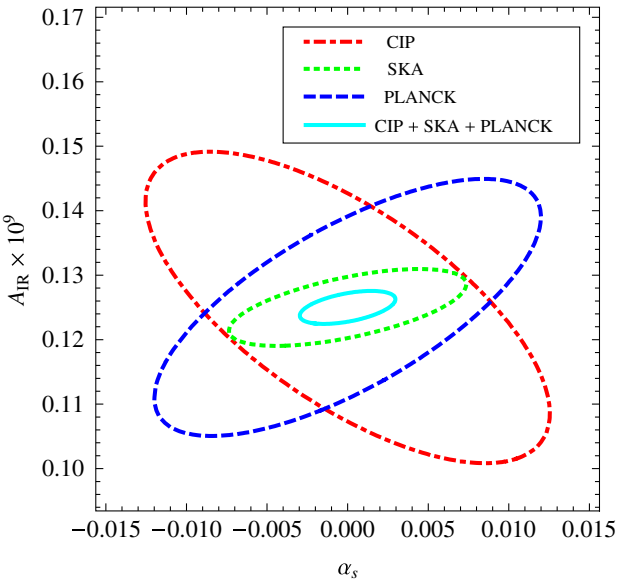


FIG. 4 (color online). Marginalized probability contours containing 68% of the posterior probability between $\alpha_s$ and $A_{\rm IR} = 1.25 \times 10^{-10}$.

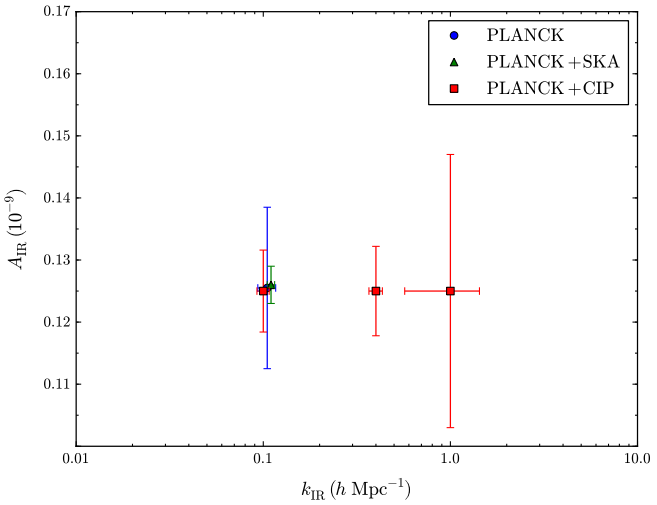


FIG. 5 (color online). The 1-$\sigma$ marginalized constraints on the amplitude and position of particle production features for Planck, Planck + SKA, and Planck + CIP. The uncertainties in $k_{\rm IR}$ are multiplied by 5 to make them more visible.

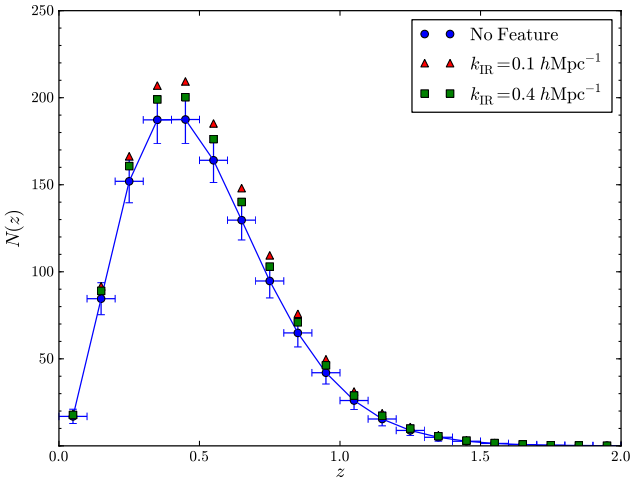


FIG. 6 (color online). The effect of a change in the primordial power spectrum on the eROSITA all-sky survey. The circles represent the number of clusters that would be observed by eROSITA for a power spectrum with no features. The triangles and squares show the excess in the number count for features at $k_{\rm IR} = 0.1$ and $0.4h$ Mpc$^{-1}$, respectively. The error bars are $1\sigma$.

Our inference of $\sigma_{A_{\rm IR}}$ and $\sigma_{k_{\rm IR}}$ is summarized in Fig. 5. As can be seen, Planck will improve the constraint at the $0.1h$ Mpc$^{-1}$ scale by about a factor of 10 in comparison to WMAP. The addition of SKA further improves the constraint by another factor of about 5. On wave numbers up to about $1.0h$ Mpc$^{-1}$, CIP combined with Planck could provide similar constraints.

Even smaller scales are constrainable, but then CIP would not be able to probe the full extent of the feature.

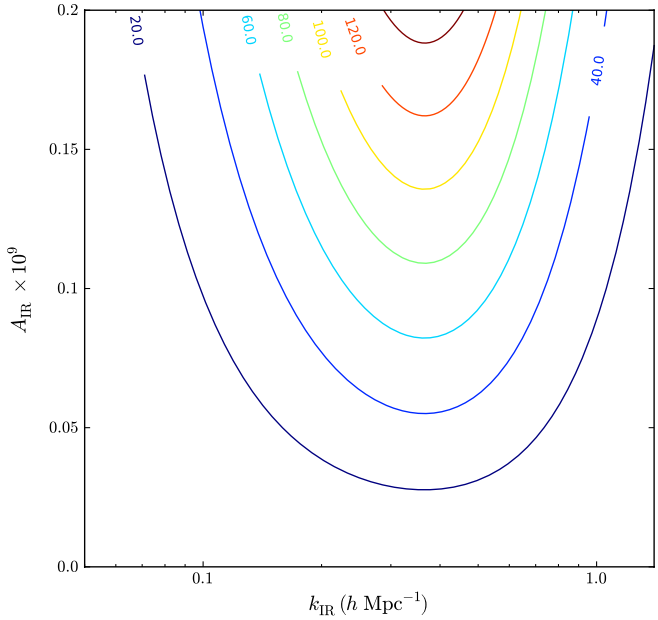


FIG. 7 (color online). The excess number count from the SNAP survey due to the feature with an amplitude $A_{\rm IR}$ and position at $k_{\rm IR}$.

Also, it may be possible to further improve the constraints by including the non-Gaussianity associated with the feature [5].

Even though the excess in cluster number counts can be easily obtained from cluster surveys (see Fig. 6 for eROSITA), they do not give better constraints in comparison to galaxies surveys partly due to low number statistics. In addition, the cluster number counts are not good at simultaneously determining the amplitude of the features and the positions due to the degeneracy in cluster counts. Because the number of clusters is determined by the integral of $P(k)$ [see Eq. (4) and (5)] the features with different amplitudes and positions can conspire to yield the same integral and, hence, number counts. Figure 7 shows the contour plot of excesses in number counts for different amplitudes and positions of the features.

In summary, we have demonstrated that future surveys can potentially probe the primordial power spectrum, for particle production-induced features, significantly more accurately and to significantly smaller length scales than at present. Even if no features are detected, at least the simplest models will have been tested much more precisely and on a much greater range of scales.

## ACKNOWLEDGMENTS

T. C. is funded by the Institute for the Promotion of Teaching Science and Technology (IPST) in Thailand. C. G. is funded by the Beecroft Institute for Particle Astrophysics and Cosmology.

[1] C. L. Bennett *et al.*, Astrophys. J. Suppl. Ser. **192**, 17 (2011).
[2] E. Komatsu *et al.*, Astrophys. J. Suppl. Ser. **192**, 18 (2011).
[3] N. Barnaby and Z. Huang, Phys. Rev. D **80**, 126018 (2009).
[4] N. Barnaby, Z. Huang, L. Kofman, and D. Pogosyan, Phys. Rev. D **80**, 043501 (2009).
[5] N. Barnaby, Phys. Rev. D **82**, 106009 (2010).
[6] J. Adams, B. Cresswell, and R. Easther, Phys. Rev. D **64**, 123514 (2001).
[7] X. Chen, R. Easther, and E. A. Lim, J. Cosmol. Astropart. Phys. 6 (2007) 023.
[8] X. Chen, R. Easther, and E. A. Lim, J. Cosmol. Astropart. Phys. 4 (2008) 010.
[9] P. Hunt and S. Sarkar, Phys. Rev. D **70**, 103518 (2004).
[10] P. Hunt and S. Sarkar, Phys. Rev. D **76**, 123504 (2007).
[11] M. Joy *et al.*, Phys. Rev. D **77**, 023514 (2008).
[12] R. N. Lerner and J. McDonald, Phys. Rev. D **79**, 023511 (2009).
[13] M. J. Mortonson *et al.*, Phys. Rev. D **79**, 103519 (2009).
[14] A. A. Starobinskij, Sov. Phys. JETP**55**, 489 (1992), http://www.jetpletters.ac.ru/ps/1276/article_19291.shtml.
[15] M. Tegmark, A. N. Taylor, and A. F. Heavens, Astrophys. J. **480**, 22 (1997).
[16] A. Jenkins *et al.*, Mon. Not. R. Astron. Soc. **321**, 372 (2001).
[17] G. Holder, Z. Haiman, and J. J. Mohr, Astrophys. J. Lett. **560**, L111 (2001).
[18] N. Kaiser, Mon. Not. R. Astron. Soc. **227**, 1 (1987).
[19] B. A. Reid, W. J. Percival, D. J. Eisenstein, L. Verde, D. N. Spergel, R. A. Skibba, N. A. Bahcall, T. Budavari, J. A. Frieman, M. Fukugita *et al.*, Mon. Not. R. Astron. Soc. **404**, L60 (2010).
[20] W. Hu and A. V. Kravtsov, Astrophys. J. **584**, 702 (2003).
[21] R. K. Sheth and G. Tormen, Mon. Not. R. Astron. Soc. **308**, 119 (1999).
[22] M. Tegmark, Phys. Rev. Lett. **79**, 3806 (1997).
[23] H. Seo and D. J. Eisenstein, Astrophys. J. **598**, 720 (2003).
[24] W. Hu and T. Okamoto, Phys. Rev. D **69**, 043004 (2004).
[25] S. Leach, Mon. Not. R. Astron. Soc. **372**, 646 (2006).
[26] M. Zaldarriaga, D. N. Spergel, and U. Seljak, Astrophys. J. **488**, 1 (1997).
[27] J. R. Bond, G. Efstathiou, and M. Tegmark, Mon. Not. R. Astron. Soc. **291**, L33 (1997).
[28] G. J. Melnick *et al.*, in Bulletin of the American Astronomical Society (2004), Vol. 36, p. 1509, http://aas.org/archives/BAAS/v36n5/aas205/311.htm.
[29] D. G. York *et al.*, Astrophys. J. **120**, 1579 (2000), http://iopscience.iop.org/1538-3881/120/3/1579/.
[30] J. R. Pritchard and E. Pierpaoli, Phys. Rev. D **78**, 065009 (2008).
[31] F. B. Abdalla, C. Blake, and S. Rawlings, Mon. Not. R. Astron. Soc. **401**, 743 (2010).
[32] P. Adshead, R. Easther, J. Pritchard, and A. Loeb, J. Cosmol. Astropart. Phys. 02 (2011) 021.
[33] M. Lampton and SNAP Collaboration, arXiv:astro-ph/0209549.
[34] G. Aldering, New Astron. Rev. **49**, 346 (2005).
[35] L. Marian and G. M. Bernstein, Phys. Rev. D **73**, 123525 (2006).
[36] W. Fang and Z. Haiman, Phys. Rev. D **75**, 043010 (2007).
[37] T. Hamana, M. Takada, and N. Yoshida, Mon. Not. R. Astron. Soc. **350**, 893 (2004).
[38] M. Takada and S. Bridle, New J. Phys. **9**, 446 (2007).
[39] S. Wang, J. Khoury, Z. Haiman, and M. May, Phys. Rev. D **70**, 123008 (2004).
[40] A. Lewis, A. Challinor, and A. Lasenby, Astrophys. J. **538**, 473 (2000).
[41] L. P. L. Colombo, E. Pierpaoli, and J. R. Pritchard, Mon. Not. R. Astron. Soc. **398**, 1621 (2009).
[42] T. Chantavat, C. Gordon, and J. Silk, Phys. Rev. D **79**, 083508 (2009).